DOI 10.1007/s10812-025-01877-2
Journal of Applied Spectroscopy, Vol. 92, No. 1, March, 2025 (Russian Original Vol. 92, No. 1, January–February, 2025)

SURFACE MORPHOLOGY AND OPTICAL AND ELECTROPHYSICAL PROPERTIES OF PIEZOCERAMIC FILMS OBTAINED BY LASER DEPOSITION IN VACUUM

N. A. Bosak,[a,*] **M. V. Bushinsky,**[b] **A. N. Chobot,**[b]
L. V. Baran,[c] **V. V. Malyutina-Bronskaya,**[d]
and I. A. Taratyn[e]

UDC 621.373.826;539.216.2

Nanostructured thin films on silicon and glass substrates have been obtained using high-frequency repetitively pulsed f ~ 10–12 kHz laser radiation with wavelength λ = 1.064 μm and power density q = 33 MW/cm^2 on a piezoceramic PZT-19 target at vacuum chamber pressure p = 2.2·10^{-2} mm Hg. The morphology of the thin piezoceramic films was studied using atomic force microscopy. Transmission spectra of the obtained films were investigated in the visible and near- and mid-IR regions. The electrophysical characteristics of PZT-19/Si structures on Si substrate were analyzed.

Keywords: *high-frequency laser irradiation, structure of thin films, transmission and reflection spectra, electrophysical characteristics.*

Introduction. Piezoceramic materials of the lead zirconate–titanate system $Pb(Ti_x,Zr_{1-x})O_3$ (PZT), which are solid solutions of lead zirconate $PbZrO_3$ and titanate $PbTiO_3$, are some of the most effective ferroelectrics. They can be prepared not only as bulk materials but also as thin films [1–4]. PZT thin films have a high dielectric permittivity, a high piezomodulus, and unique electrooptical properties. The piezo- and ferroelectric properties of PZT films depend on their formation technology. The ability to form thin ferroelectric films on metallic, semiconductor, and dielectric substrates opens broad possibilities for constructing functional electronic devices, facilitating the formation in one technological process of both functional ferroelectric elements and signal processing devices [5–11]. The preparation technology of thin-film solid solutions is based on various methods, e.g., chemical deposition from solutions and the vapor phase, laser deposition of aerosols, sol-gel processes, and magnetron sputtering [1, 3, 7, 12]. Crystallization is an important stage of film formation. For this, isothermal or rapid thermal annealing at temperatures from 473 to 1023 K is used. As a result, a film crystallizes from an amorphous state to form a perovskite phase that has ferroelectric properties through an intermediate phase with the pyrochlore structure [13]. It is noteworthy that the market volume for ultrathin piezoelectric MEMS sensors based on PZT and aluminum nitride (AlN) is growing every year, including because of wide use in the automotive industry [14]. The composition and structure of the obtained materials must be studied for successful use of materials based on thin films. Preparation and study of the PZT/Si structure are critical to the use of these films in microelectronics.

The present work studied PZT-19 piezoceramic thin films deposited in vacuum onto silicon and glass substrates using high-frequency repetitively pulsed laser radiation [15]. The morphology of the obtained thin films was studied using electron and atomic-force microscope. Transmission spectra in the near- and mid-IR regions and reflection spectra in the visible and near-IR regions were characterized. The voltammetric (VAC) and volt–Faraday characteristics (VFC) were studied.

[*]To whom correspondence should be addressed.

[a]B. I. Stepanov Institute of Physics, National Academy of Sciences of Belarus, Minsk, Belarus; email: n.bosak@ifanbel.bas-net.by; [b]SSPA Scientific and Practical Center of the National Academy of Sciences of Belarus for Materials Science, Minsk, Belarus; email: bushinsky@physics.by; [c]Belarusian State University, Minsk, Belarus; email: baran@bsu.by; [d]SSPA Optics, Optoelectronics and Laser Technology, Minsk, Belarus; email: malyutina@oelt.basnet.by; [e]Belarusian National Technical University, Minsk, Belarus. Translated from Zhurnal Prikladnoi Spektroskopii, Vol. 92, No. 1, pp. 59–64, January–February, 2025. Original article submitted July 11, 2024.

Experimental. Piezoceramic films were deposited using high-frequency laser sputtering of a ceramic target in a vacuum ($p = 2.2 \cdot 10^{-2}$ mm Hg). The experimental laser setup (λ = 1.06 μm) with the laser pulse repetition rate regulated from 5 to 50 kHz contained a laser-radiation source, optical system for transporting laser radiation to the target being sputtered, a vacuum chamber, and a measurement-diagnostic module. The laser pulse repetition rate was changed by varying the pump laser level and gate optical density from an irradiated LiF crystal with F_2^- color centers. The laser pulse length at half height was τ ~ 85 ns. Macroscopically homogeneous thin films were deposited at laser radiation power density q = 33 MW/cm^2 and pulse repetition rate f ~ 10–12 kHz.

The elemental compositions of the target and film were obtained using energy-dispersive x-ray spectroscopy (EDX) and an SEM EVO 10 scanning electron microscope with a microfocus x-ray spectral analyzer (Oxford Instruments Nanotechnology Tools Ltd.).

The surface morphology of PZT films prepared on silicon and glass substrates was studied using scanning electron (SEM EVO 10 microscope) and atomic-force microscopy (AFM) using a Solver P47 PRO scanning probe microscope. Contactless silicon cantilevers with hardness coefficient 3.1 N/m, resonance frequency 140 kHz, and probe roundness radius <10 nm were used for AFM. The surface morphology was studied in amplitude–frequency modulation mode at constant force. Transmission of optical radiation by thin films in the near-IR region was measured on a Cary 500 Scan spectrophotometer. Transmission spectra in the mid-IR region were recorded using a NEXUS FIR spectrometer (Thermo Nicolet) in the range 400–4000 cm^{-1}. VAC and VFC were measured using an E7-20 automated immitance meter at room temperature. VFC were measured at signal frequencies 100 and 500 kHz and 1 MHz.

Results and Discussion. Table 1 presents the elemental compositions of the target and film in wt.% and at.% that were obtained using EDX. Figure 1 shows the areas of the target and film surfaces from which the results were obtained. The results agreed well with the target–film compositions.

Figure 2 shows the sample surface from electron microscopy at magnification 500× and 5000×. The surface had sharply pronounced relief (Fig. 2a) consisting of round formations up to 5 μm in size. In turn, the round formations were formed by separate nanometer-sized particles, which is visible in Fig. 2a at magnification 5000×. Cracks were observed on the surface under an optical microscope. The average film thickness measured under the optical microscope was 5.5 μm.

Figure 3 shows AFM images of the surface of PZT films prepared on silicon and glass substrates. AFM showed that a developed film surface with a large variety of structural elements of various shapes and sizes formed upon deposition of films onto glass and silicon substrates. For example, formations of closed and open rings and elongated formations were found besides large spherical particles of diameter 1–5 μm. Scanning of an area 5 × 5 μm revealed that the film also consisted of a finely disperse phase with small structural elements varying in size from 50 to 300 nm. The average height of the surface relief of PZT films prepared on silicon and glass substrates was 880 nm with a mean-square roughness of 384.2 nm.

The transmission coefficient of the silicon substrate increased sharply to T = 52.8% at λ = 982 nm and remained practically unchanged up to λ = 2500 nm (Fig. 4a). The transmission coefficient in the near-IR region of the laser-deposited piezoceramic film on silicon was T = 34.8% at λ = 1155 nm, increasing smoothly to T = 47.1% at λ = 2500 nm.

Two absorption bands at ν = 607.4 and 1107 cm^{-1} with the transmission coefficient reaching a constant T = 53.8% in the range 1200–3783 cm^{-1} were observed in the transmission spectrum of the silicon substrate in the mid-IR region (Fig. 4b) [16]. The transmission coefficient of the PZT film on the silicon substrate increased sharply from T = 6.1% at ν = 403 cm^{-1} to T = 34.9% at ν = 1232 cm^{-1} with T = 36.4–38.2% in the range 1232–3783 cm^{-1}.

The reflection spectrum of the silicon substrate (Fig. 4c) exhibited two maxima at λ = 243.2 and 369.1 nm and a broad band from λ = 460.0 nm (R = 24.9%) to λ = 1021 nm (R = 28.8%), which was characteristic of single-crystalline silicon [16]. The reflection coefficient of the piezoceramic film on the silicon substrate R = 4.8–9.0% in the range 200–1098 nm.

The transmission coefficient of the glass substrate in the visible and near-IR regions (Fig. 4d) increased sharply from T = 0.2% at λ = 298 nm to T = 87% at λ = 358 nm and remained constant up to λ = 2622 nm. The transmission spectrum of the laser-deposited piezoceramic film on the glass substrate exhibited two areas of growth and almost constant transmission T = 27% in the range 1549–2685 nm.

The dependence of the transmission coefficient of the glass substrate in the mid-IR spectral region (Fig. 4e) contained two steps. The transmission of the piezoceramic film increased sharply from T = 0.95% at ν = 2119 cm^{-1} to T = 18% at ν = 2514 cm^{-1} and from T = 12.9% at ν = 3567 cm^{-1} to T = 21.8% at ν = 3708 cm^{-1}. The shape of the transmission spectrum in the mid-IR region of the PZT film on the glass substrate repeated the shape of the transmission spectrum of the

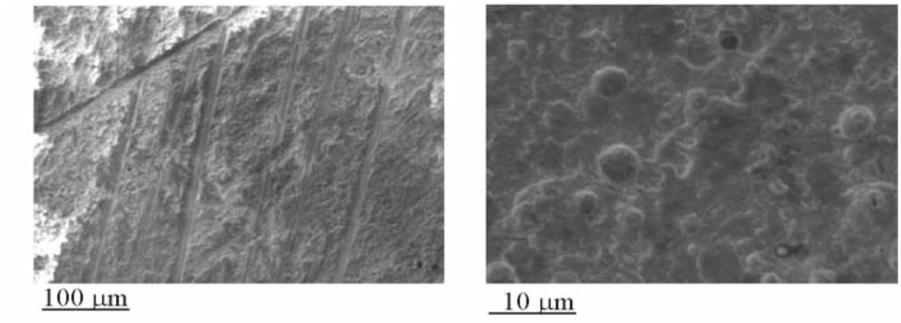

Fig. 1. Areas of target (a) and film (b) from which EDX data were obtained.

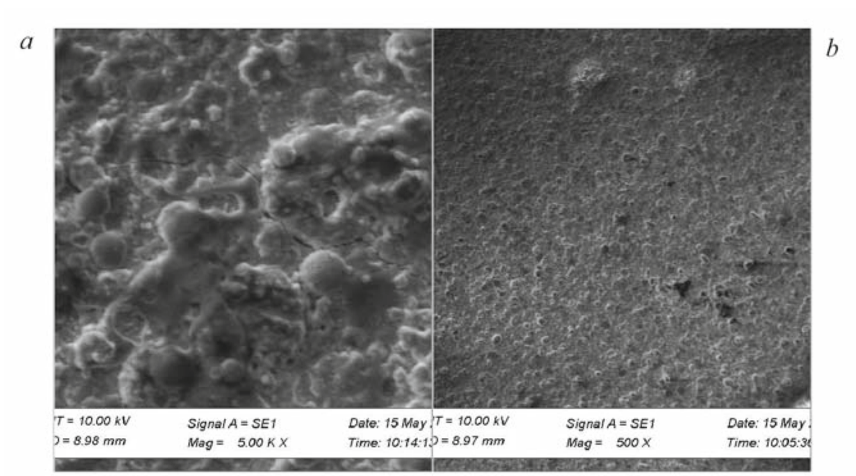

Fig. 2. Film surface morphology at magnification 5000× (a) and 500× (b).

TABLE 1. Elemental Composition of Target and Film

Element	Target composition		Film composition	
	wt.%	at.%	wt.%	at.%
C	4.80	21.62	3.57	17.54
O	13.91	47.06	12.57	46.30
Ti	6.46	7.30	7.10	8.74
Zr	13.47	7.99	15.41	9.96
Pb	61.36	16.03	61.34	17.45
Total	100.00	100.00	100.00	100.00

glass substrate. However, the transmission coefficient of the PZT film in the range 2514–3567 cm^{-1} varied from 10 to 15% because of absorption in the film.

Two maxima were observed in the reflection spectrum of the glass substrate with R = 6.3% at λ = 204.2 nm and R = 7.7% at λ = 352.7 nm. The reflection coefficient of the PZT thin film (Fig. 4f) reached a maximum R = 6.3% at λ = 190.7 n and a minimum R = 2.9% at λ = 1095 nm. The reflection spectrum $R(\lambda)$ exhibited two maxima at 309 and 650 nm.

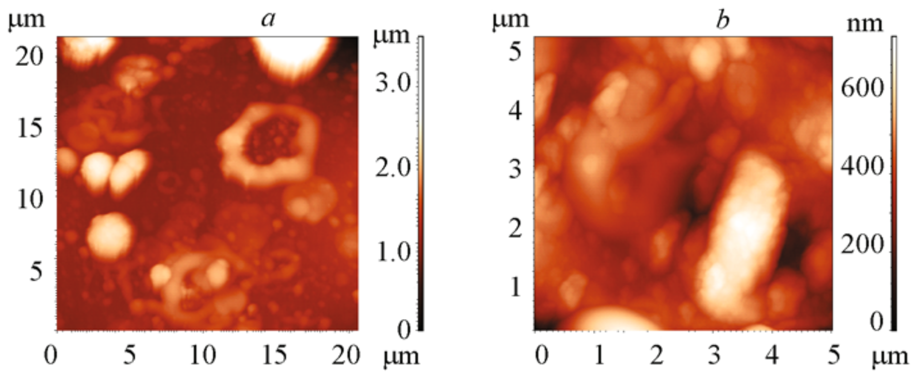

Fig. 3. AFM images of surface of laser-deposited thin piezoceramic film on silicon (a) and glass (b) substrates.

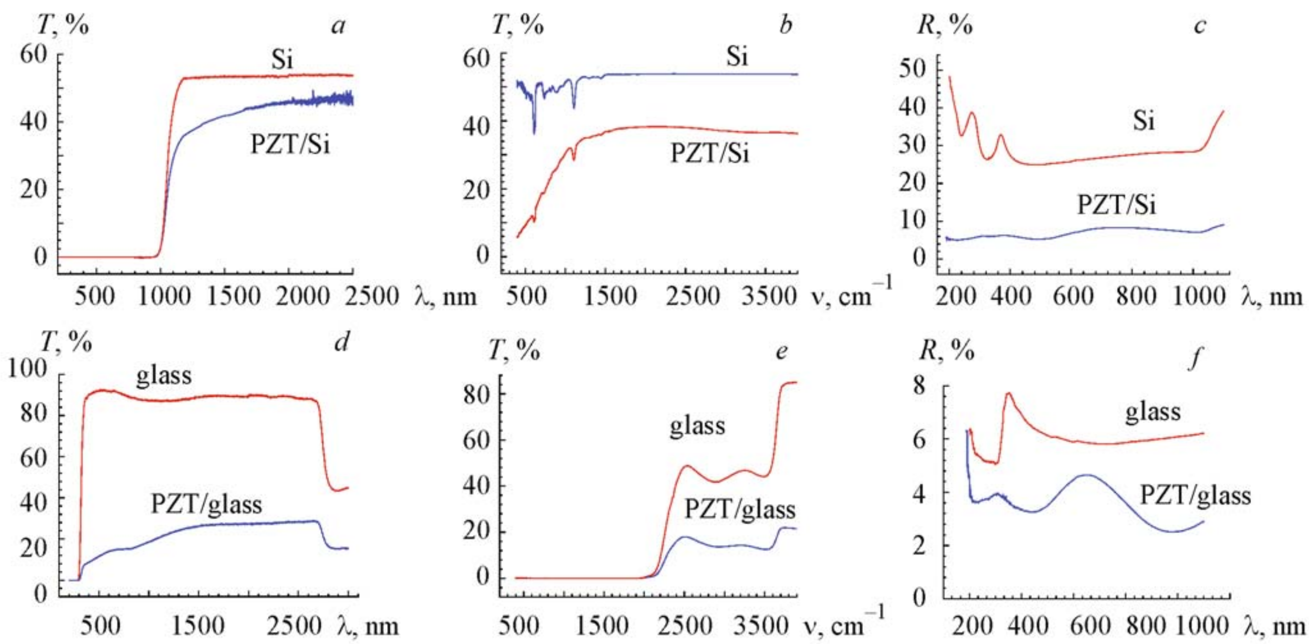

Fig. 4. Transmission spectra in the visible, near- (a, d), and mid-IR regions (b, e) and reflection spectra (c, f) of laser-deposited piezoelectric film on silicon (a, b, c) and glass (d, e, f) substrates.

Figure 5a shows the VAC of the PZT/Si structure. The polarity of the potential in the VAC corresponded to the polarity of the potential applied to the PZT film. The dependence of the current on the applied potential was asymmetric. The ratio of the currents for positive and negative potentials of 15 V was 2.16. This asymmetry of the VAC could be attributed to the different values of the potential barriers localized at the lower and upper film interfaces upon polarization. Figures 5c, d, and e show the VAC in linear, Mott, and Poole–Frenkel coordinates, respectively [17]. The VAC were linear in the potential range from 0 to 1.5 V and from 0 to –5 V (Fig. 5c), which was consistent with an ohmic mechanism of conductivity. Figure 5d shows a linear dependence of the VAC for potentials from 1.5 to 9 V and from –5 to –9 V, which suggested a Poole–Frenkel conductivity mechanism, according to which the type of potential barriers for charge carriers between atoms of the crystal lattice changed with these electric fields applied to the structure. The VAC were linear in Mott coordinates at positive and negative potentials >9 V (Fig. 5d). This indicated that the dominant conductivity mechanism at these potentials was by space-charge limited current (SCLC) [18].

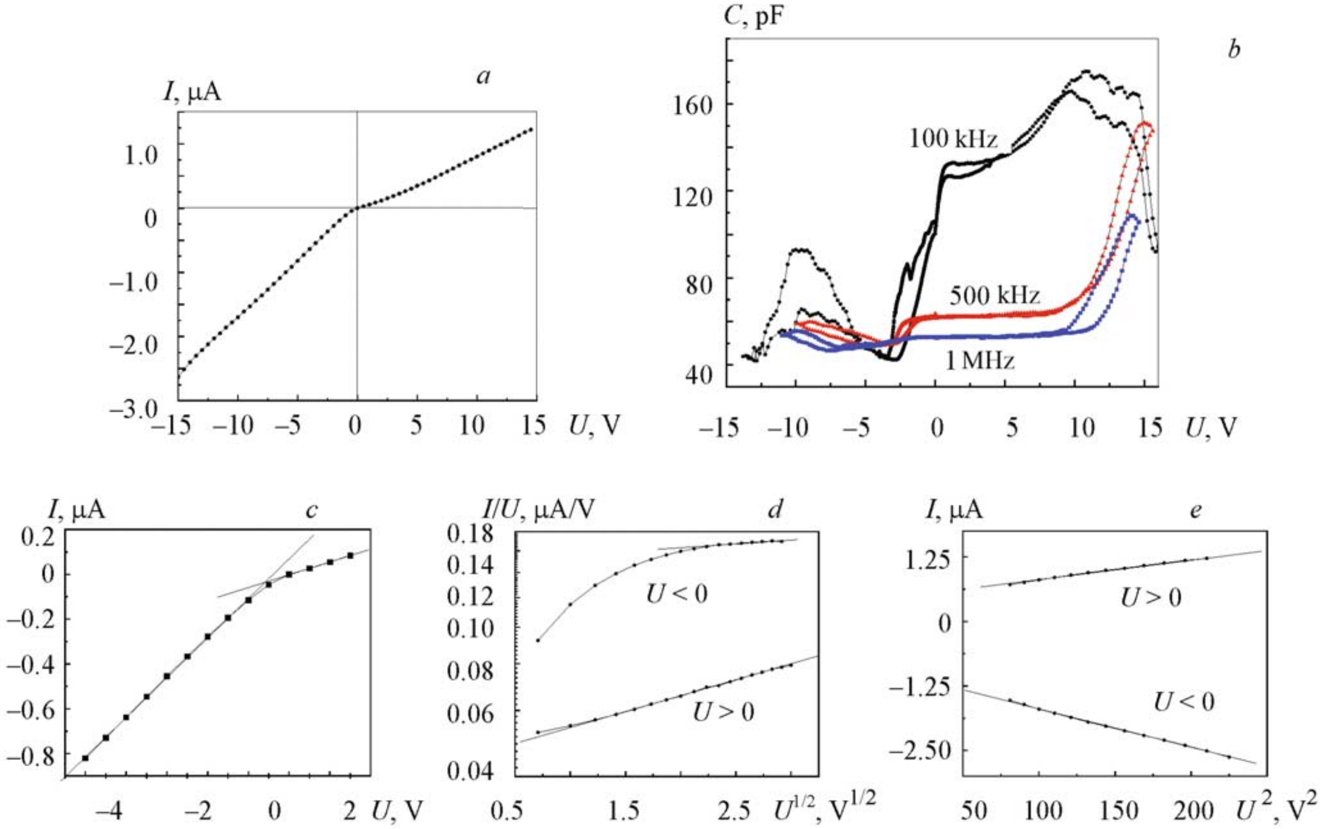

Fig. 5. Voltammetric (a) and volt–Faraday (b) characteristics of PTZ/Si structures and representation of VAC in linear (c), Mott (d), and Poole–Frenkel (e) coordinates.

Figure 5b shows the VFC of the PZT-19/Si structure that were measured at frequencies 100 kHz, 500 kHz, and 1 MHz. Several peculiarities were observed in the characteristics, e.g., a maximum near potential −10 V and a step in the function of the signal frequency in the potential range from −5 to 0 V. The capacitance was observed to vary as a function of the frequency. The maximum of the capacitance at potential −10 V decreased with increasing frequency of the measuring signal. The hysteresis of the step and its height decreased. The capacitance dropped at positive potentials. The hysteresis at frequencies 100 kHz, 500 kHz, and 1 MHz were 4, 1.1, and 1.7 V, respectively.

The presence of hysteresis at positive potentials indicated that the studied structures demonstrated a charge response that could be explained by the presence of ferroelectric phases and charge defects. Considering that Pb is highly reactive with Si and easily diffuses into silicon substrates, generation of an extended defect region with a broad energy spectrum of surface states at the PZT-19/Si interface could be proposed. This could explain the presence of the maximum and the steps at negative potentials. The shape of the VFC (Fig. 5b) could also be explained by the SiO_x interphase layer being capable of reducing the total capacitance and the actual potential applied to the ferroelectric and by the strong electric field applied to the SiO_x interface, which often causes significant problems with charge injection [7].

Conclusions. High-frequency laser sputtering of a ceramic target in vacuum formed films of $Pb(Ti_x,Zr_{1-x})O_3$ with a developed surface morphology on silicon and glass substrates. The elemental composition of the film correlated with that of the target. The average height of the film surface relief was 880 nm with a mean-square roughness of 384.2 nm. The reflection coefficient of the piezoceramic film on the silicon substrate was R = 4.8–9% in the range 200–1098 nm. The electrical properties of the unannealed PZT-19/Si structure were determined by uncompensated charges of the ferroelectric phases and charge defects in the film and at the PZT-19/Si interface. An analysis of the VAC showed that the PZT-19/Si structure characteristically had several conductivity mechanisms, i.e., ohmic (at low potentials from 0 to 1.5 V and from 0 to −5 V), Poole–Frenkel emission (from 1.5 to 9 V and from −5 to −9 V), and space-charge limited current (at potentials greater than ±9 V).

REFERENCES

1. S. Baba, H. Tsuda, and J. Akedo, *IEEE Trans. Ultrason. Ferroelectr. Freq. Control*, **55**, No. 5, 1009–1016 (2008).
2. K. Y. Choi, T. S. Kim, D. K. Choi, J. Y. Park, and D. S. Yoon, *Integr. Ferroelectr.*, **69**, No. 1, 93–101 (2005).
3. S. K. Pandey, A. R. James, C. Prakash, T. C. Goel, and K. Zimik, *Mater. Sci. Eng., B*, **112**, No. 1, 96–100 (2004).
4. V. V. Petrov, Y. N. Varzarev, A. S. Kamentsev, A. A. Rozhko, and O. A. Pakhomova, *Nano Hybrids Compos.*, **28**, 65–70 (2020).
5. L. S. Jang and K. C. Kuo, *Sensors*, **7**, No. 4, 493–507 (2007).
6. S. R. Krishnamoorthi, K. S. Venkatesh, and R. Ilangovan, *Adv. Condens. Matter Phys.*, **2013**, 1–6 (2013).
7. S. R. Krishnamoorthi, K. S. Venkatesh, and R. Ilangovan, *J. Ovonic Res.*, **9**, No. 3, 81–88 (2013).
8. J. Hong, H. W. Song, S. Hong, H. Shin, and K. No, *J. Appl. Phys.*, **92**, 7434–7441 (2002).
9. N. Izyumskaya, Y. I. Alivov, S. J. Cho, H. Morkoc, H. Lee, and Y. S. Kang, *Crit. Rev. Solid State Mater. Sci.*, **32**, Nos. 3–4, 111–202 (2007).
10. G. D. Shilpa, K. Sreelakshmi, and M. G. Ananthaprasad, *IOP Conf. Ser.: Mater. Sci. Eng.*, **149**, Article ID 012190 (2016).
11. T. Ito, T. Nishi, T. Umegaki, H. Hida, and I. Kanno, *J. Phys.: Conf. Ser.*, **1052**, Article ID 012094 (2018).
12. B. Beklesovas, A. Iljinas, V. Stankus, J. Cyviene, M. Andrulevicius, M. Ivanov, and J. Banys, *Coatings*, **12**, 717 (2022).
13. A. M. Solodukha, I. E. Shramchenko, A. M. Khoviv, and V. A. Logacheva, *Fiz. Tverd. Tela*, **49**, No. 4, 719–722 (2007).
14. *Express Information on Foreign Electronics Technology*, No. 17 (6691), Aug. 29, 2019 (2019).
15. L. Ya. Min′ko, A. N. Chumakov, and N. A. Bosak, *Kvantovaya Élektron. (Moscow)*, **17**, No. 11, 1480–1484 (1990).
16. A. N. Magunov and O. V. Lukin, *Mikroelektronika*, **25**, No. 2, 97–111 (1996).
17. V. N. Igumnov, *Physical Principles of Microelectronics: Textbook* [in Russian], 2nd edn., Mariiskii Gos. Tekh. Univ., Ioshkar-Ola (2010).
18. M. V. Kamenshchikov, A. V. Solnyshkin, A. A. Bogomolov, and I. P. Pronin, *Fiz. Tverd. Tela*, **53**, No. 10, 1975–1979 (2011).